Analytical modelling of the trans-scale cutting forces in diamond cutting of polycrystalline metals considering material microstructure and size effect

Zhanwen Sun[a], Tao Zhang[a], Peizheng Li[a], Sujuan Wang[a,b,*], Suet To[c], Hailong Wang[a]

[a] *State Key Laboratory of Precision Electronic Manufacturing Technology and Equipment, Guangdong University of Technology, Guangzhou, China*

[b] *Guangdong Provincial Key Laboratory of Micro-Nano Manufacturing Technology and Equipment, School of Electromechanical Engineering, Guangdong University of Technology, Guangzhou, China*

[c] *State Key Laboratory in Ultra-precision Machining Technology, Department of Industrial and Systems Engineering, The Hong Kong Polytechnic University, Kowloon, Hong Kong*

* Corresponding author Email：grace.wangsj@gdut.edu.cn

Abstract

In diamond cutting of polycrystalline metals, the influence of size effect and microstructure on the cutting force is prominent due to the trans-scale variation of undeformed chip thickness (UDCT) from microscale to nanoscale. This study proposes a trans-scale cutting force model for diamond cutting of polycrystalline metals with the full consideration of microstructure, material elastic recovery, size effect and round-tool-edge effect. Specifically, by corelating micro-forming theory and crystal plastic theory, a hybrid slip-line model (HSLM) is developed to determine the flow stress in the primary deformation zone, which can quantify the influence of size effect and microstructure, such as grain size, grain boundary and crystal anisotropy, on flow stress. Then, the normal cutting force and frictional cutting force are determined by analyzing the stress distribution and frictional states at tool-chip interface using a tool-chip contact model. The rubbing force induced by material elastic recovery at very small UDCT is determined based on indentation theory. Through diamond cutting of polycrystalline copper with different grain sizes, it is experimentally demonstrated that the proposed HSLM can capture the cutting mechanism transformation phenomenon from shearing (tensile stress) to ploughing (compressive stress) with increasing size factor. Besides, the proposed force model has the improved estimation accuracy compared with the conventional force models developed based on Johnson-Cook constitutive equation.

Keywords: Diamond cutting process; Analytical force model; Trans-scale cutting mechanism; Size effect; Microstructure of polycrystalline metals

Nomenclature	η	Size factor

Symbol	Description	Symbol	Description
$o_w\text{-}x_w y_w z_w$	Coordinate system built on workpiece	$\sigma_s\ \sigma_i$	Flow stress of surface grains and inner grains
$o_t\text{-}x_t y_t z_t$	Coordinate system built on tool center point	$N_s\ N_i\ N_t$	Grain numbers of surface layer, inner layer and whole workpiece
τ_R	Critical resolved shear stress	D	Grain size
k	Grain boundary related stress	D'	Size effect coefficient
$\sigma\ \varepsilon\ \dot{\varepsilon}$	Stress, strain and strain rate	ϕ_i	Shear angle
$k_R\ n$	Coefficients related to critical resolved shear stress	$M\ m$	Orientation factors for polycrystal and single crystal
$A\ B\ C\ p\ q$	Parameters of Johnson-Cook equation	$T_w\ T_m\ T_0$	Working temperature, melting temperature and room temperature
$\tau_s\ \gamma_s\ \dot{\gamma}_s$	Equivalent flow stress, strain and strain rate	ζ	Coefficient related to equivalent tool-chip contact length
γ_e^i	Equivalent tool rake angel	l_{AB}	Length of shear band
γ_0	Tool rake angle	C_0	Coefficient related to strain rate
v_{sh}^i	Velocity along shear band	t_c^i	Undeformed chip thickness
v	Cutting speed	r_e	Tool edge radius
$a\ b$	Coefficients related to shear angle	β	Friction angle
ρ	Density of the workpiece	S	Specific heat in cutting region
θ	Angle between the resultant force and shear band	$\sigma_A^i\ \sigma_B^i$	Hydrostatic flow stress at point A and B
β'	Heat dissipation coefficient	$v_\perp$	Velocity vertical to shear band
$s_1\ s_2$	Distance parallel and vertical to the shear band	s	Distance along equivalent tool rake face
l_c^i	Tool-chip contact length	l_s^i	Length of the chip sticking region
r	Coefficient related to tool-chip contact length	j	Coefficient characterize the pressure distribution
μ_f	Friction coefficient on tool rake face	$F_n^i\ F_f^i$	Nominal cutting force and frictional cutting force

$F_{c,s}^i\ F_{t,s}^i$	Cutting force and thrust force for the i-th discrete element	ψ_i	Inclination angle between the equivalent rake face and z-axis
x_i	Coordinate of the i-th discrete element	Λ_i	Tool-workpiece interference volume
κ	Tool clearance angle	w_i	Width for the i-th discrete element
d_c	Critical depth of cut	k_r	Rubbing force coefficient
μ_r	Friction coefficient of rubbing	$F_c^i\ F_t^i$	Total cutting and thrust force
R	Tool nose radius	d	Depth of cut
N	Number of discrete elements	$\sigma_n^i\ \sigma_f^i$	Distribution of normal and frictional stress

1. Introduction

Ultra-precision diamond cutting is widely regarded as a promising technology to fabricate optical components and precision moulds, due to its capability to achieve submicron form accuracy and nanometric surface roughness [1]. For example, Sun et al. [2] employed a self-tuned diamond cutting system to efficiently fabricate infrared micro-optics arrays with high form accuracy. To better design the diamond cutting process, it is of great importance to investigate the efficient modelling methods of cutting force with high accuracy, as the prediction of cutting force is the premise of optimizing cutting parameters [3], understanding material removal mechanism [4] and suppressing tool tip vibration [5]. Besides, cutting force model is the basis for some innovative machining technologies such as forced-controlled servo cutting, in which cutting force serves as the feedback signal of the tool servo motion to improve the machining accuracy of freeform surfaces [6]. Dai et al. [7] investigated the relation between the cutting force and the center cone generation in diamond turning, based on which an intelligent tool setting error compensation strategy is developed with high efficiency. In diamond cutting, the depth of cut (DoC) is generally comparable with the gain size, and the undeformed chip thickness (UDCT) can change from a few nanometers to tens of micrometers along the round cutting edge [8]. At this range, the tool-workpiece engagement area covers a few grains or even a single grain of the workpiece material. Hence, material microstructure, such as grain size, grain boundary and crystal anisotropy, has a strong impact on the cutting mechanism and the micro-mechanics properties of the workpiece material, leading to the difficulty to accurately predict the cutting force in diamond cutting of polycrystalline metals.

However, up to now, few studies have focused on the modelling of the diamond cutting force with the full consideration of the trans-scale variation UDCT and the material microstructure.

According to the employed modelling theory, the current force models basically consist in two types, namely empirical models and analytical models. For example, Huang et al. [9] proposed an empirical cutting force model for diamond turning by considering tool edge radius effect and material elastic recovery. Without fully understanding the internal cutting mechanism, empirical models generally require a large number of early experiments to determine the force coefficients, which is low efficient and has relatively weak applicability in other cutting conditions. In contrast, analytical models derived by deeply analyzing the tool-workpiece interactions and material removal mechanism are more scientific and practical, and has drawn a widespread attention by researchers [10, 11]. An analytical force model of elliptical vibration cutting was proposed by Lin et al. [12] through investigating the transient variation of chip thickness and shear angle. Zhu et al. [13] investigated the dynamic cutting forces generated in slow tool servo turning using both analytical and finite element modelling methods. Recently, an analytical cutting force model of micro-milling process was proposed by Wojciechowski et al. [14] with the consideration of the chip formation accumulation phenomenon, which achieves better estimation accuracy with conventional models. Wan et al. [15] proposed an analytical model describing the material separation process in micro-milling together with the influence of minimum uncut chip thickness, based on which a cutting force model is proposed considering both shearing and ploughing effect. Through analyzing the cutting forces during laser-assisted machining of WC/NiCr clad layer, Przestacki et al. [16] proposed an efficient method to estimate the minimum uncut chip thickness. At present, current analytical models have developed by thoroughly incorporating dynamics, plastic mechanics, thermal physics and friction actions, thereby achieving relatively high estimation accuracy of cutting forces for turning [17] and milling [18] processes. However, these models are still unreliable to predict the cutting force for diamond cutting featuring a trans-scale variation of UDCT from microscale to nanoscale, due to the insufficient understanding of the influence of microstructure on cutting mechanism.

In diamond cutting, the tool engages with only a few or even one grains of the workpiece material, and only a fraction of the grains is removed by the tool edge. At this cutting process, the forward motion of the tool tip serves as a strong source of cracks and dislocations, inducing the plastic deformation of the workpiece material along shear band. Through successive sliding of the dislocations from one grain to another, lamella-like chips are formed according to Merchant's slip-line model [19]. When the UDCT

further reduces to submicron-scale or even nanoscale, dislocation sliding together with size effect becomes the key role in affecting the flow stress, resulting in the transition of stress from tensile (shearing mechanism) to compressive (ploughing mechanism) [20]. The stress-strain relationship of polycrystalline metals under micro-deformation is shown in Fig. 1, where microstructures including grain size, grain boundary, dislocation density are the significant factors that influence the stress [21, 22]. Thus, the complicated micro-mechanics of polycrystalline metals leads to the difficulty on modelling the cutting force for diamond cutting, and the correlation of microstructure on the determination of flow stress is necessary to improve the predicting accuracy.
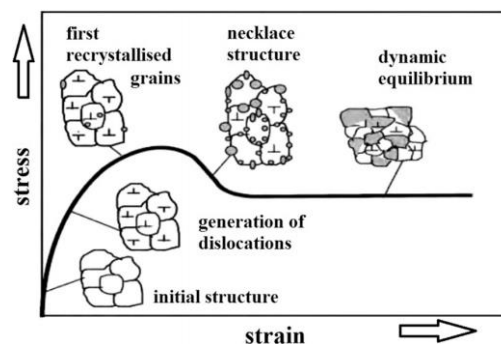
Fig. 1. The influence of microstructure on material stress-strain relationship [21].

With the significant scaling down of the UDCT in diamond cutting, size effect that relates to the special micro-mechanics of the workpiece material becomes increasingly prominent for influencing the material removal mechanism. Size effect refers to the phenomenon that when the dimensions of the workpieces are scaled down to a certain value, the physical behaviors and mechanical response of the workpieces greatly changes [23]. For example, by applying nanoindentation on different metal alloys, Prasitthipayong et al. [24] and Kim et al. [25] found that the hardness of metal alloys greatly increases with the decrease of indentation size, named as indentation size effect. Size effect majorly results from the remarkable reduction of the grain numbers in the deformation zone, in which case individual grains become crucial and the macroscope mechanics principles may be inapplicable [26]. In other words, the size effect results from the increasingly prominent of the influence of material microstructure on plastic deformation with the scaling down of the workpiece dimensions. Chen et al. [27] experimentally studied the size effect in micro-milling, and found that size effect has a significant impact on the surface roughness in case that the ratio of feed rate to tool edge radius is lower than a critical value. To provide a theoretical explanation on size effect, a surface layer model was proposed by Lai et al. [28]. The uniqueness of this model is the incorporation of a size factor into the Armstrong's model to describe the different mechanics properties between the surface layer and inner layer. They suggested that the

reduction of the flow stress with the minimization of specimen is attributed to the less restriction of the dislocation sliding in the surface layer grains. Recently, Zhang et al. [29] investigated the influence of size effect on the surface generation in diamond fly cutting, and suggested that the difference of the strain energy between the surface layer grain and inner layer grain induces the unwanted surface rough patterns on the machined surface. Overall, it is learned that size effect plays a key role in diamond cutting. However, few research works have been proposed on how the size effect quantitatively affects the cutting force in diamond cutting of polycrystalline metals.

In analytical modelling of cutting force, slip-line theory is generally used to analyze the chip formation and material removal process in cutting zone [30]. Currently, slip-line models have developed from macroscope to microscope by considering equivalent negative rake angle at small DoC and by ever-refining the shear band. For example, Fang et al. [31] proposed a slip-line model featuring curved shear band to account for the curled chip formation mechanism and the chip back-flow behavior in cutting process. Similarly, Ke et al. [32] theoretically demonstrated the saw-tooth chip formation mechanism by in-depth investigating the shear-slip geometry of the slip-line field. To model the extrusion force in micro-cutting, Ren et al. [33] reported an extend slip-line model that detailly describes the flow direction of the trapped metal beneath the cutting edge. Hu et al. [34] proposed a modified slip-line model by considering the equivalent negative rake angle, tool-chip friction and thermal distribution in micro-cutting process. However, the current slip-line models generally employ the famous Johnson-Cook constitutive equation to estimate the flow stress in primary deformation zone, which cannot reflect the impact of microstructure and size effect on the material deformation. Especially, these slip-line field approaches cannot well explain the high compressive flow stress (extrusion mechanism) and the resulting 'powder-like' chips generated in micro-cutting at small DoC [20]. Therefore, a comprehensive slip-line model that fully considers the negative rake angle, microstructure, size effect is required to be proposed, so as to deeply understand the chip formation mechanism and to accurately estimate the flow stress and trans-scale cutting forces.

As mentioned above, diamond cutting features a trans-scale variation of UDCT from microscale to nanoscale, in which case the increasingly prominent microstructure coupled with size effect lead to the difficulty on efficiently estimate the trans-scale cutting force with high accuracy. Facing this dilemma, an analytical force model is proposed in this study for predicting the diamond cutting force with the full consideration of the microstructure of polycrystalline metals and size effect. Based on the Oxley's model

[35, 36], a hybrid slip-line model (HSLM) is, for the first time, developed to present the influence of equivalent negative rake angle, grain size, grain boundary, dislocation sliding and size effect on the stress distribution in the deformation zone. The rubbing force induced by the material elastic recovery at very small UDCT is determined based on indentation theory. In consideration of the trans-scale variation of UDCT along cutting edge, discrete and summation methods are employed to calculated overall cutting force. To validate the proposed force model, diamond cutting experiments were conducted on polycrystalline copper with different grain sizes. Besides, the generated chip morphologies are analyzed to validate the advantage of the proposed HSLM on determining the flow stress transition phenomenon with decreasing UDCT.

2. Trans-scale cutting force model for diamond cutting

Before modelling the cutting force, the engaged region of the cutting edge is equally discretized into *N* independent orthogonal cutting pieces. The influence of microstructure and size effect on the plastic flow stress in the primary deformation zone is quantitatively studied through proposing a hybrid slip-line model (HSLM). Then, the normal cutting force and frictional cutting force at the tool-chip interface are determined through analyzing the stress distribution and tool-chip contact state in the secondary deformation zone. For the discrete element having very small UDCT, the rubbing force induced by material elastic recovery is calculated based on indentation theory. Finally, the force components of each discrete elements are summarized to determine the overall cutting force and thrust forces. The details are introduced as follows.

2.1 Cutting force model considering microstructure and size effect

In case that the UDCT is larger than the minimum uncut chip thickness, normal cutting force and frictional cutting force are generated at the tool-chip interface attributing to the material plastic deformation along shear band.

2.1.1 Hybrid slip-line model

As learned from metal sheet micro-forming theory, the ratio of grain size to sheet thickness has a strong correlation with the material micro-mechanics properties during plastic deformation [37]. Similarly, in the scenario of ultra-precision diamond cutting, size factor (SF) defined as the ratio of the grain size to UDCT greatly influence the cutting mechanism and flow stress when the cutting scale drops from millimeters to micrometers or even nanometers. To accurately calculate the size factor dependent flow stress, a HSLM describing micro/nano-cutting of polycrystalline metals is proposed on the basis of

Oxley's model by fully considering the microstructure and size effect, as shown Fig. 2. A coordinate system o_w-$x_w y_w z_w$ is fixed on the workpiece with y-axis is in accordance with the cutting direction. The feature of the proposed hybrid model is the division of the workpiece into two layers according to the UDCT, namely surface layer (shaded by yellow) and inner layer (shaded by pink). In micro/nano-cutting process, the surface layer grains are compressed by the tool rake face, resulting in the plastic deformation of the workpiece material along shear band as well as the formation of the chip at the too-chip interface.
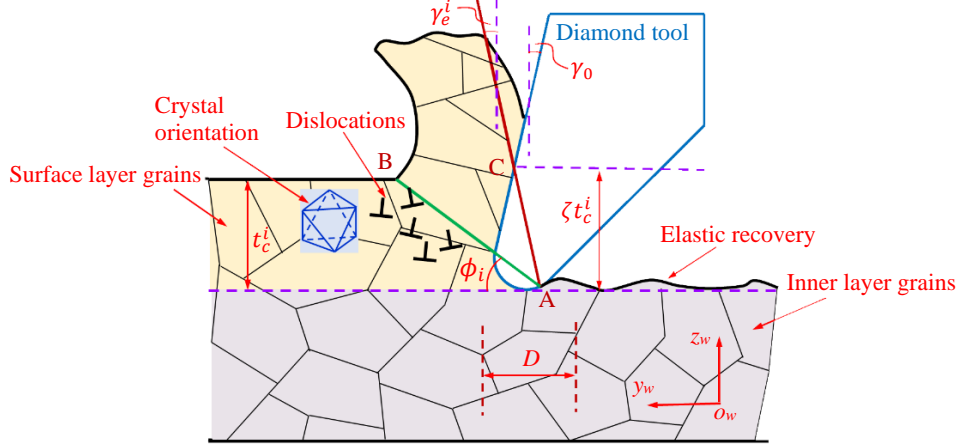
Fig. 2. Schematic of the hybrid slip-line model considering microstructure and size effect.

According to the 'surface layer model', the grains located in the cutting region is less restricted than the ones inside the workpiece [28]. Besides, the share of the surface grains increases with the increase of size factor, so the flow stress (σ) of the deformed material can be formulated by

$$\sigma = \frac{N_s \sigma_s + N_i \sigma_i}{N_t} = \eta \sigma_s + (1 - \eta) \sigma_i \tag{1}$$

where N_s and N_i represent the number of the grains in the surface layer and inner layer; N_t is the total grain number. σ_s and σ_i denote the flow stress of surface grains and inner grains, respectively, and η is size factor. According to crystal plastic theory and the famous Hall–Petch equation, the mechanics properties of the surface layer grains is similar to single crystal, while that of inner layer grains similar to polycrystal [28]. Therefore, the flow stress of the surface layer grains and inner layer grains can be expressed by

$$\sigma_s = m \tau_R(\varepsilon) \tag{2}$$

$$\sigma_i = M \tau_R(\varepsilon) + \frac{k}{\sqrt{D}} \tag{3}$$

where m and M are the orientation factors that represent the effect of crystal anisotropy for single crystal and polycrystal, respectively. k represent the necessary stress required to propagate general yield across the polycrystal grain boundaries, which is determined by the dislocation density. D is the grain size.

Thereby, the second term of Eq. (3) corelates the microstructure to flow stress. $\tau_R(\varepsilon)$ denote the critical resolved shear stress for single crystal, which can be expressed as an exponential function of strain rate $k_R \varepsilon^n$ according to crystal plastic theory [23]. Hence, the quasi-static flow stress of deformed material in micro/nano-cutting can be expressed by combining the size dependent and size independent parts as

$$\sigma(\varepsilon) = \left(M k_R \varepsilon^n + \frac{k}{\sqrt{D}} \right) - \eta \left(M k_R \varepsilon^n + \frac{k}{\sqrt{D}} - m k_R \varepsilon^n \right) \tag{4}$$

It is worth to note that Eq. (4) describe the stress-strain relation of polycrystalline metals under quasi-static deformation. With the consideration of the strain rate and thermal effect, the constitutive relation of workpiece material can be described by the well-known Johnson-Cook equation, in which the flow stress is formulated as a product of three terms representing the effect of strain, strain rate and working temperature, respectively, as the following equation

$$\sigma(\varepsilon) = [A + B\varepsilon^p] \left[1 + C \ln\left(\frac{\dot{\varepsilon}}{\varepsilon_0} \right) \right] \left[1 - \left(\frac{T_w - T_0}{T_m - T_0} \right)^q \right] \tag{5}$$

The first term in Eq. (5) is designed as $A + B\varepsilon^p$ to make the stress-strain curve fitting easier, where the coefficients of A and B relate to yield strength and strain-hardening modulus, but it cannot represent the influence of microstructure and size effect on the quasi-static flow stress. For the second term, the effect of strain rate on flow stress is addressed through introducing strain-rate coefficient C. The third term represents the influence of working temperature, and T_m, T_0 and T_w denote the melting temperature, room temperature and working temperature, respectively. p and q are the coefficients relating to strain hardening and thermal softening, respectively. ε_0 is reference plastic strain-rate equaling to 1.

Generally, Johnson-Cook constitutive equation is limited to estimate the flow stress in macroscopic plastic deformation. According to Ran et al. [23], difficult-to-eliminate deviation will generates when Johnson-Cook equation is used as the stress-strain fitting formula for micro/nanoscopic plastic deformation. Therefore, the $A + B\varepsilon^p$ term in Johnson-Cook equation is replaced by Eq. (4) in this study, to corelate the microstructure and size effect to the flow stress estimation. Besides, another size effect coefficient D' is also imported to amend strain rate with respect to size effect. With the assistance of the well-known Von Mises Criterion, the equivalent flow stress (τ_s), strain (γ_s) and strain rate ($\dot{\gamma}_s$) in cutting region can be related to the flow stress (σ), strain (ε) and strain rate ($\dot{\varepsilon}$) in Johnson-Cook equation. Thus, the constitutive relation of polycrystalline metals in micro/nano-deformation is expressed as

$$\tau_s(\varepsilon) = \frac{1}{\sqrt{3}} \left[\left(M k_R \left(\frac{\gamma_s}{\sqrt{3}} \right)^n + \frac{k}{\sqrt{D}} \right) - \eta \left(M k_R \left(\frac{\gamma_s}{\sqrt{3}} \right)^n + \frac{k}{\sqrt{D}} - m k_R \left(\frac{\gamma_s}{\sqrt{3}} \right)^n \right) \right]$$

$$\left[1 + C\,ln\left(\frac{\dot\gamma_s}{\sqrt{3}}\right)\right]\left[1 + D'ln\left(\frac{\eta}{\eta_0}\right)\right]\left[1 - \left(\frac{T_w - T_0}{T_m - T_0}\right)^q\right] \tag{6}$$

where η_0 is the reference size factor for macroscopic deformation. According to Ref [38], the strain in the shear band for the i-th discrete element can be assumed as a constant value and expressed as

$$\gamma_s^i = \frac{cos\gamma_e^i}{2sin\phi_i cos(\phi_i - \gamma_e^i)} \tag{7}$$

where γ_e^i and ϕ_i represent the equivalent rake angle and shear angle for the i-th discrete element. The corresponding strain rate ($\dot\gamma_s^i$) can be estimated by adopting Oxley's empirical expression [36], whose availability has been proven in the force modelling for micro-cutting process and can be expressed as

$$\dot\gamma_s^i = \frac{C_0 v_{sh}^i}{l_{AB}} = \frac{C_0 v_{sh}^i sin\phi_i}{t_c^i} \tag{8}$$

where C_0 is the factor that relates to the material property and cutting condition. l_{AB} is the length of the straight shear band and t_c^i denote the practical UDCT at the i-th discrete element. According to the geometrical relation in Fig. 2, the velocity along the shear band (v_{sh}^i) for the i-th discrete element is formulated as

$$v_{sh}^i = \frac{cos\gamma_e^i}{cos(\phi_i - \gamma_e^i)} v \tag{9}$$

where v denote the cutting speed. In micro/nano-cutting, the extreme small UDCT makes the equivalent rake angle to be highly negative. According to [38, 39], the original round tool edge can be replaced by an equivalent tool rake face in micro-cutting, though drawing a straight line between the point A and C as shown in Fig. 2. Point A is the contact point between the bottom of the tool edge and the machined surface, and the point C located on tool rake face is the mark point of the equivalent tool-chip contact length. Thus, based on the geometrical relation, the equivalent rake angle (γ_e^i) at a specific UDCT can be determined by

$$\gamma_e^i = \gamma_0 + arctan\left(\frac{u_i}{\zeta t_c^i}\right) \tag{10}$$

$$u_i = \begin{cases} r_e cos\gamma_0 - \dfrac{\zeta t_c^i - r_e}{cos\gamma_0} & t_c^i \geq \dfrac{r_e(1 + sin\gamma_0)}{\zeta} \\ r_e cos\left(arcsin\left(\dfrac{r_e - \zeta t_c^i}{r_e}\right)\right) & esle \end{cases} \tag{11}$$

where r_e denotes the tool edge radius and γ_0 is the tool rake angle. ζ is the coefficient that determines the equivalent tool-chip contact length.

Shear angle is jointly influenced by the cutting condition and the material property [30]. Especially in micro/nano-cutting, the impact of crystal anisotropy on shear angle cannot be neglected, because the tool-workpiece normally interacts within a single crystal. Wang et al. [40] theoretically and experimentally demonstrated that the activated dislocation slip system in the primary deformation zone depends on the relative angle between the cutting direction and the crystal orientation. Thus, to address the crystal anisotropy, a modified shear angle equation is proposed in this study by incorporating Taylor factor (M), which is normally used as an approximate measure of the relative direction of dislocation sliding activities to the crystal orientation, into Lee's shear angle equation as

$$\phi_i = (aM + b)\left(\frac{\pi}{4} + \gamma_e^i - \beta\right) \tag{12}$$

where a and b are the constant for the linear relation, which can be derived by curve fitting method. β denotes the friction angle.

The working temperature (T_w) in the deformation zone is required to be estimated before calculating flow stress using Eq. (6). As it is difficult to accurately measure the working temperature using experimental methods, analytical models are generally regarded as an alternative way. Even though mathematical and finite element methods have been reported to determine the temperature distribution in micro/nano-cutting process, these models can greatly complicate the force model [41, 42]. To improve the modelling efficiency, a simplified Boothroyd's temperature model [43] is proposed in this study to calculate the working temperature, and it can be expressed by

$$T_w = T_0 + \frac{2(1 - \beta')\gamma_s^i \tau_s}{\rho S} \tag{13}$$

where β' denotes the heat dissipation coefficient, ρ is the density of the workpiece material and S is the specific heat. This proposed temperature estimation model fully considers the plastic deformation heat, thermal diffusion and heat convection. By incorporating Eq. (7), Eq. (8) and Eq. (13) into the Eq. (6), the shear flow stress that acts parallel to the shear band can be analytically determined.

2.1.2 Calculation of nominal and frictional cutting force

The cutting force is essentially generated by the interactions between tool rake face and chip, so the distribution of flow stress at the secondary deformation zone (tool-chip interface) needs to be determined before calculating the nominal cutting force and frictional cutting force. As shown in Fig. 3, according to the stress equilibrium relation in the shear band, the change rate of hydrostatic stress along the straight line AB can be expressed by Ref [35]

$$\frac{\partial \sigma}{\partial s_1} = \frac{\partial \tau}{\partial s_2} = \frac{\partial \tau}{\partial \gamma}\frac{\partial \gamma}{\partial t}\frac{\partial t}{\partial s_2} + \frac{\partial \tau}{\partial \dot{\gamma}}\frac{\partial \dot{\gamma}}{\partial s_2} + \frac{\partial \tau}{\partial T_w}\frac{\partial T_w}{\partial s_2} \tag{14}$$

where s_1 and s_2 are the distance parallel and vertical to the shear band. According to [13], the temperature gradient is small enough to be neglectable, and the strain rate can be assumed to approach the maximum value at the shear band. Thus, the second term and the third term are assumed to be equal to zero, and the hydrostatic stress at point A for the i-th discrete element can be calculated by integral method as

$$\sigma_A^i = \sigma_B^i + \frac{t_c^i}{v_\perp sin\phi_i}\frac{\partial \tau_s}{\partial \gamma_s^i}\dot{\gamma}_s^i \tag{15}$$

where $v_\perp$ is the velocity vertical to the shear band equal to $vsin\phi_i$ and the term $\frac{\partial \tau_s}{\partial \gamma_s^i}$ can be obtained through conducting differential algorithm on Eq. (6) as

$$\frac{\partial \tau_s}{\partial \gamma_s^i} = \frac{\sqrt{3}[(1-\eta)M + \eta m]\sqrt{D}k_R n {\gamma_s^i}^{n-1}\tau_s}{(1-\eta)\left[\sqrt{D}Mk_R{\gamma_s^i}^{n} + (\sqrt{3})^{n}k\right] + \eta m k_R {\gamma_s^i}^{n}} \tag{16}$$
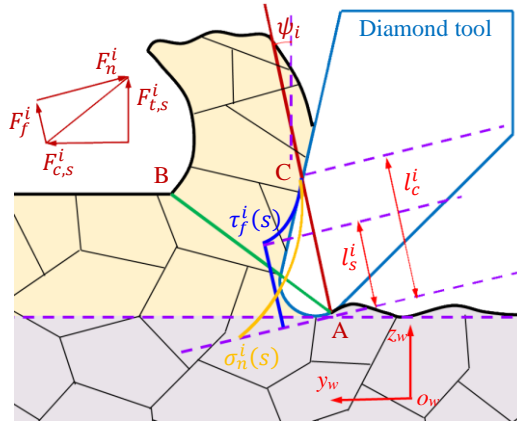

Fig. 3. Schematic of the normal and frictional stress distribution at tool-chip interface.

As the cutting direction is parallel to the original surface of the workpiece, the boundary condition of flow stress can be obtained by Oxley's approximate cutting theory, in which the strain, strain rate and temperature along line AB are assumed to be constant [36]. Thus, the change rate of the hydrostatic stress along shear band is also constant according to Eq. (14), and another expression between the hydrostatic stress of point A and point B can be expressed by

$$\sigma_A^i + \sigma_B^i = 2\tau_s tan(\theta) \tag{17}$$

where θ is the angle between the resultant force and shear band, which can be estimated by Ref. [44]

$$tan(\theta) = 1 + 2\left(\frac{\pi}{4} + \phi_i\right) - \frac{t_c^i}{2\tau_s sin\phi_i}\frac{\partial \tau}{\partial s_2} \tag{18}$$

Through integrating Eq. (17) into Eq. (15), the hydrostatic stress of point A (σ_A^i) and point B (σ_B^i) can be determined. In orthogonal cutting, the normal stress (σ_n^i) at the equivalent tool-chip interface exponentially decreases from the highest value at point A (σ_A^i) to zero at the tool-chip separation point C, as the yellow line shown in Fig. 3. Accordingly, the distribution of the normal stress at equivalent tool-chip interface can be expressed as

$$\sigma_n^i(s) = \sigma_A^i \left[1 - \left(\frac{s}{l_c^i} \right)^j \right] \tag{19}$$

where s denotes the coordinate along equivalent tool rake face with respect to point A, and j is the coefficient that characterizes the shape of the stress distribution. l_c^i denotes the tool-chip contact length for the i-th discrete element. It is worth to note that the equivalent tool-chip interface is defined as the straight line connecting the bottom of the cutting edge (point A) and the tool-chip separation point (point C). According to the momentum equilibrium, the contact length l_c^i can be expressed by Ref. [45, 46]

$$l_c^i = \frac{2 + r}{r} \frac{t_c^i \cos(\phi_i + \beta - \gamma_e^i)}{\sin\phi_i \cos\beta} \tag{20}$$

In diamond cutting, the tool-chip contact state is very complicated featuring discontinuous frictional states of sticking and sliding, as shown in Fig. 3. Specifically, in the region near the bottom of cutting edge, the high normal stress exerted on the tool leads to the sticking friction state with constant frictional stress. With the decrease of the normal stress in the region near the tool-chip separation point, the frictional state transfers to the sliding govern by the Coulomb friction law. Even though the hybrid analytical-numerical models proposed in previous studies are high qualified for the estimation of the discontinuous frictional state at tool-chip interface [47], these models can reduce the efficiency of the cutting force model. Besides, it is still difficulty for current analytical models to determine the location of the transfer point from sticking the sliding. Thus, a simplified tool-chip contact model is proposed in this study to efficiently estimate the discontinuous distribution of the frictional stress (σ_f^i) at tool-chip interface, which is expressed as

$$\sigma_f^i(s) = \begin{cases} \mu_f \sigma_A^i \left[1 - \left(\frac{l_s^i}{l_c^i} \right)^j \right] & 0 \leq s < l_s^i \\ \mu_f \sigma_n^i(s) & l_s^i \leq s < l_c^i \end{cases} \tag{21}$$

where μ_f is the friction coefficient and l_s^i denote the length of sticking region. According to the model, frictional stress is increasing when approaching to the bottom of the cutting edge. Based on the plastic deformation criterion, the frictional stress should be no larger than the hydrostatic stress at the exit of the

shear band (point B) [36]. Accordingly, the length of the sticking region can be obtained by the following expression as

$$l_s^i = l_c^i \left(1 - \frac{\sigma_A^i}{\mu_f \sigma_B^i}\right)^{\frac{1}{j}} \tag{22}$$

Through integration method, the nominal cutting force and frictional cutting force for the i-th discrete element can be estimated as

$$F_n^i = \int_0^{l_c^i} w_i \sigma_n^i(s)ds \tag{23}$$

$$F_f^i = \int_0^{l_c^i} w_i \sigma_f^i(s)ds \tag{24}$$

Overall, the cutting force and thrust force for the i-th discrete element can be obtained by coordinate transformation as

$$F_{c,s}^i = F_n^i sin\psi_i + F_f^i cos\psi_i \tag{25}$$

$$F_{t,s}^i = F_n^i cos\psi_i - F_f^i sin\psi_i \tag{26}$$

where ψ_i is the induced angle between the equivalent tool rake face and vertical direction, and can be determined according to the geometrical relation in Fig. 3 as

$$\psi_i = \begin{cases} arccos\left(\dfrac{l_c^i}{2r_e}\right) & l_c^i < 2r_e sin\left(\dfrac{\pi}{4} + \dfrac{\gamma_0}{2}\right) \\ arcsin\left(\dfrac{r_e + r_e sin\gamma_0}{l_c^i}\right) - \gamma_0 & else \end{cases} \tag{27}$$
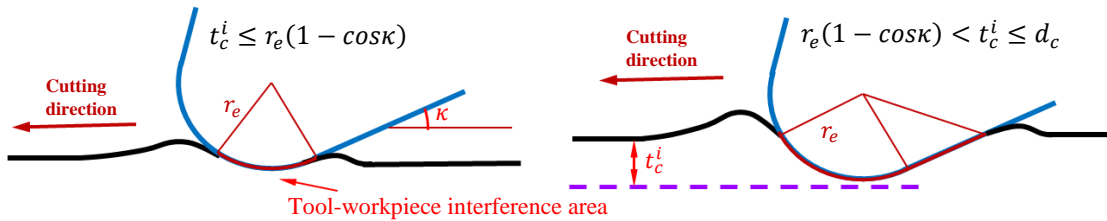
Fig. 4. Schematic of the tool-workpiece interference area for rubbing force.

2.2 Rubbing force model

The minimum uncut chip thickness that defines the critical threshold of UDCT affecting the initiation of chip formation has a strong impact on the cutting mechanism in ultra-precision diamond cutting. When the undeformed chip thickness is lower than the minimum uncut chip thickness, the workpiece material only experiences elastic deformation and flows beneath the tool edge, instead of plastic decohesion [14]. In this case, the material is extruded beneath the tool edge similar to indentation operation, as illustrated in Fig. 4. Accordingly, the rubbing force can be assumed to be proportional to

the interference volume between the cutting edge and workpiece [48, 49]. With the consideration of the tool geometrical shape and the width of discrete element, the interference volume (Λ_i) for the i-th discrete element can be calculated as

$$\Lambda_i = \begin{cases} 2w_i r_e \arccos\left(\dfrac{r_e - t_c^i}{r_e}\right) & t_c^i \leq r_e(1 - cos\kappa) \\ w_i r_e \arccos\left(\dfrac{r_e - t_c^i}{r_e}\right) + r_e\kappa + \dfrac{t_c^i - r_e(1 - cos\kappa)}{sin\kappa} & r_e(1 - cos\kappa) < t_c^i \leq d_c \end{cases} \tag{28}$$

where d_c denote the critical DoC and is assumed to be $r_e(1 - cos\xi)$, where ξ characterize the angular position of the critical DoC and is approximately equal to 0.75, according to Ref [30]. The rubbing force induced by the material elastic deformation in cutting direction ($F_{c,r}^i$) and thrust direction ($F_{t,r}^i$) for the i-th discrete element can be expressed by

$$F_{c,r}^i = \mu_r \Lambda_i k_r \tag{29}$$

$$F_{t,r}^i = \Lambda_i k_r \tag{30}$$

where μ_r denotes the friction coefficient of rubbing and k_r is the rubbing force coefficient that can be determined by assuming that the rubbing force and cutting force is continuous at the minimum uncut chip thickness.
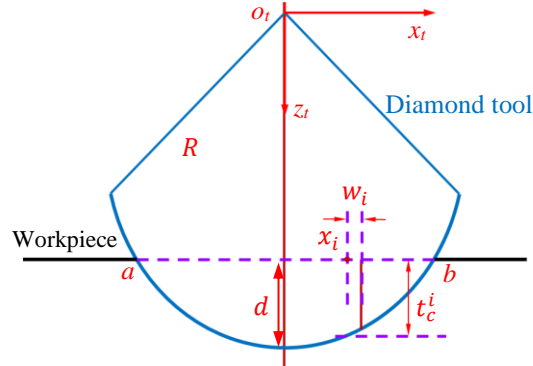

Fig. 5. Schematic of the tool-workpiece engagement area.

2.3 Force model for diamond sculpturing

Fig. 5 schematically shows the tool-workpiece engagement area at a specific DoC of d. A coordinate system o_t-$x_t z_t$ is built on the center of round cutting edge with the z-axis vertical to the workpiece. As shown in Fig. 5, the engagement area is symmetric with respect to the z-axis, so the coordinates of x_a and x_b can be expressed as

$$x_a = -x_b = \sqrt{R^2 - (R - d)^2} \tag{31}$$

where R denotes tool nose radius. The engagement area is evenly divided along x-axis to obtain N discrete orthogonal cutting elements. The relative position (x_i) as well as the corresponding undeformed chip thickness (t_c^i) and width (w_i) and the of the i-th discrete element can be expressed as

$$x_i = x_a + i\frac{2x_b}{N} \tag{32}$$

$$t_c^i = \sqrt{R^2 - x_i^2} - R + d \tag{33}$$

$$w_i = \frac{2Rarcsin\frac{x_b}{R}}{N} \tag{34}$$

In total, by summarizing the force components of all the discrete elements as expressed in Eq. (25), Eq. (26), Eq. (29) and Eq. (30), the overall cutting force and thrust force generated in diamond cutting of polycrystalline copper at a specific DoC of dc can be calculated by

$$\begin{cases} F_c^i = \sum\{F_{c,r}^i | \forall t_c^i < d_c\} + \sum\{F_{c,s}^i | \forall t_c^i \geq d_c\} \\ F_t^i = \sum\{F_{t,r}^i | \forall t_c^i < d_c\} + \sum\{F_{t,s}^i | \forall t_c^i \geq d_c\} \end{cases} \tag{35}$$

3. Experiment setup

To validate the proposed force model, orthogonal cutting experiments were conducted in this study using Moore 350FG multi-axis ultra-precision lathe, as shown in Fig. 6. The workpiece with plane surface is screwed on a fixture, and then sticked on the locked spindle. A single crystal diamond tool (Contour Company) is mounted on a force sensor (Kistler 9256C), and then configured on the z-slide of the lathe. As illustrated in Fig. 7, through feeding the diamond tool along Y-axis with a preset DoC, a micro-groove can be fabricated on the workpiece. In this way, the cross-sectional surface of the fabricated micro-groove is in accordance with the shape of the cutting edge, as shown in Fig. 6. A large span of DoCs ranging from 0.3 μm to 15 μm were adopted in the experiments, to sufficiently verify the general applicability of the proposed model for trans-scale cutting process. The cutting speed is fixedly set at 30 mm/min. The cutting edge radius is measured at 40 nm by Atomic Force Microscopy (AFM). The flank face of the diamond tool is designed in conic shape, to ensure the uniformity of the clearance angle along cutting edge. The rake angle and clearance angle of the tool is 0° and 7°, respectably. The tool nose radius is 0.5 mm. To accurately capture the cutting force signal, the experiments were conduced under dry cutting condition, and the sample frequency of the force sensor is set at 30 KHz. After cutting experiments, the formed chips are collected and observed by scanning electron microscope (SEM), to study the trans-scale cutting mechanism.
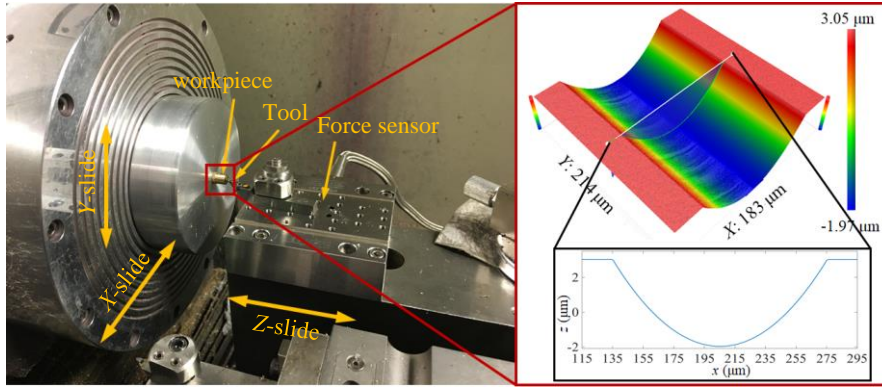
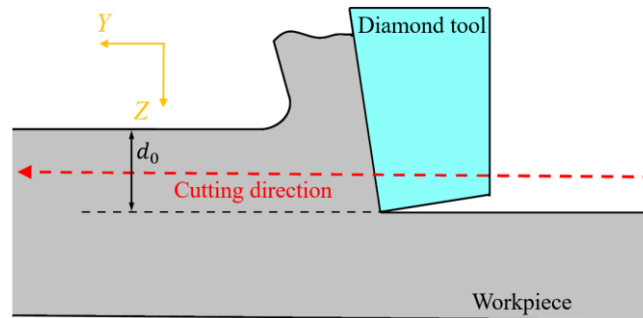**Fig. 6.** Experiment setup for diamond cutting and the machined micro-groove.

Fig. 7. Illustration of the kinematics of the micro-groove cutting.

Polycrystalline copper is used as the workpiece material in this study. To determine the influence of grain size on the cutting force, it is necessary to conduct cutting experiments on the polycrystalline copper workpiece with different grain sizes. Thus, the workpiece material is heat treated to obtain vary microstructure. After heat treatment, the workpiece material is etched and observed using an optical microscope (BX60, Olympus corporation) to measure the average grain size. The average grain size of the two samples employed in this study is 24 μm and 52 μm, respectively. It is worth to note that the elemental component of the workpiece material basically remains unchanged before and after the heat treatment [20]. This justify the scientificity of the cutting experiments for investigating the influence of grain size on cutting force.

4. Results and discussion

In this section, to understand the trans-scale cutting mechanism in diamond cutting of polycrystalline metals, the difference of the cutting mechanism between macro-cutting and micro/nano-cutting is analyzed based on the proposed model. Then, the capability of the proposed HSLM on capturing the cutting mechanism transformation from shearing (tensile stress) and ploughing (compressive stress) is validated by correlating the simulation results and the chip morphologies. Finally, the effectiveness of the proposed trans-scale cutting force model is validated by comparing the estimated

forces and the experimentally measured forces in diamond cutting of polycrystalline copper with different grain sizes.

4.1 Correlation of trans-scale cutting mechanism and size factor

According to Eq. (33), the trans-scale variation of the UDCT along cutting edge under different DoCs can be determined and is shown in Fig. 8 (a). Herein, the engaged cutting edge is equally discretized into 50 pieces to better present the variation trend. It is observed that the UDCT decreases from the tool tip (in the middle of the tool edge) to the two sides of the engaged region, due to the round cutting edge of the diamond tool. The largest UDCT reached at the tool tip is equal to the practical DoC, while the UDCT near the two sides is reduced to a few nanometers. The changes of the UDCT of the 5th, 15th and 25th discrete elements with the increase of DoC are shown in Fig. 8 (b). According to the proposed model, each discrete element of the cutting edge is treated as an independent orthogonal cutting section with corresponding local UDCT. Thus, it is learned that diamond cutting features a trans-scale variation of UDCT from tens of micrometers to a few nanometers, and the local UDCT of each discrete element is jointly dependent on its position on the tool edge and the adopted DoC.
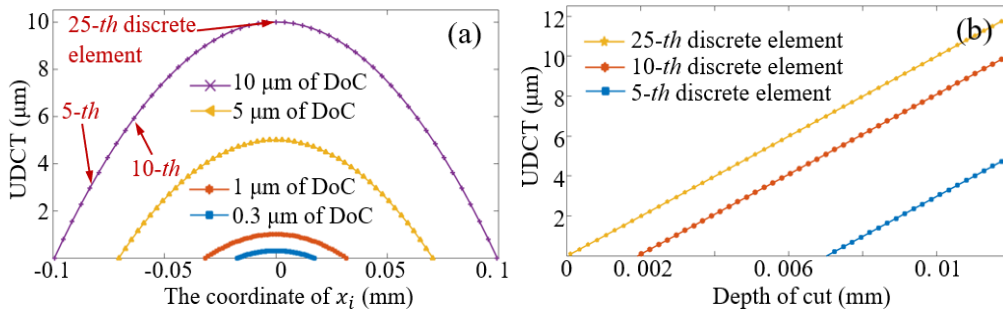

Fig. 8. The variation of UDCT (a) along cutting edge at the DoC of 10 μm, 5 μm, 1 μm, 0.3 μm and (b) for the 5-*th*, 10-*th* and 25-*th* discrete element with increasing DoC.
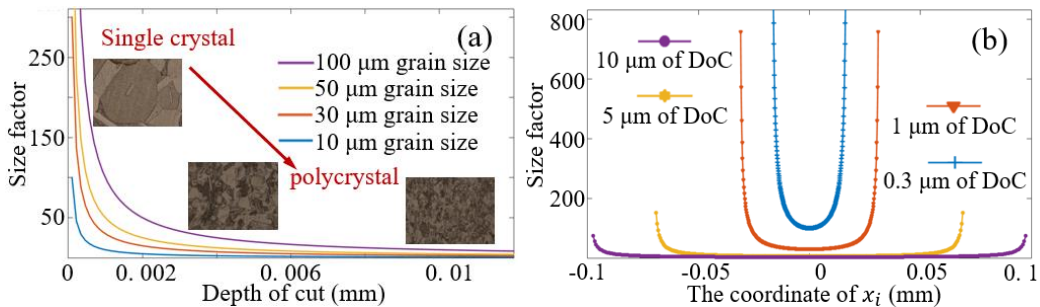

Fig. 9. The variation of size factor (a) with increasing DoC for the grain size of 100 μm, 50 μm, 30 μm, 10 μm and (b) along cutting edge at the DoC of 10 μm, 5 μm, 1 μm, 0.3 μm.

It is known from literature that when the UDCT decreases from micrometers to nanometers, the cutting mechanism changes from shearing with tensile stress to ploughing with compressive stress [20]. According to metal sheet micro-forming theory, this cutting mechanism transformation phenomenon can

be described by the index of size factor (SF) defined as the ratio of the grain size to UDCT. As shown in Fig. 9 (a), SF decreases with the increase of UDCT, and the average SF increases with the increase of the grain size. According to the definition of SF, smaller SF means that more crystals are included in the cutting region, similar to macro cutting of polycrystals. The variation of SF along cutting edge at different DoCs is shown in Fig. 9 (b), which is corresponding to Fig. 8 (a). It is seen that SF increases from the tool tip to the two sides of the tool edge, and the average SF value of the whole cutting edge also increases with the decrease of DoC. As learned from Fig. 9 (a), the increase of SF with decreasing UDCT indicates that less crystals are included in the cutting region, in which case the influence of microstructure factors (i.e., grain size, grain boundary, crystallographic anisotropy, micro-cracks, dislocation evolution) on material micro-mechanics properties become increasingly prominent during material plastic deformation, similar to micro/nano cutting of single crystals. Besides, as learned for 'Surface layer model', the surface grains in the cutting region suffer less deformation resistance than that of internal grains, as the few dislocations pile up at free surface, further leading to lower flow stress in the deformation zone under large SF [26].

As discussed above, diamond cutting of polycrystalline metals features a trans-scale cutting mechanism including shearing of macro-cutting and ploughing of micro/nano-cutting, due to the large variation of SF at different positions of cutting edge. In this case, the influence of microstructure and size effect on the flow stress during material removal should be considered in the modelling of cutting force, in order to accurately estimate the cutting forces generated in both macro- and micro/nano-cutting process.

4.2 Validation of the proposed hybrid slip-line model

In this section, the chip morphologies formed in diamond cutting of polycrystalline copper under different DoCs are analyzed by SEM to further elucidate the effect of SF variation on the trans-scale cutting mechanism. As shown in Fig. 10 (a), with a DoC of 10 μm, intensive lamella-like structures are observed on the free surface of the chip as pointed by the red arrows. As learned from macro-cutting mechanism, the lamella-like structures are generated by the adiabatic shear band (ASB)-dominated material removal mechanism under tensile stress (shearing mechanism) [50]. It is interesting to observe that the density of the lamella-like structures is weakening from the middle to the two sides of the chip when the DoC decreases to 5 μm and 1 μm, as shown in Fig. 10 (b) and (c). Especially, no lamella-like structures are observed on the two sides of the chips with a DoC of 1 μm and 0.3 μm as marked by the

green circles, as shown in Fig. 10 (d). Besides, the chips generated with a DoC of 0.3 μm is very thin and fragile. This indicates that the material near the two sides of the chip is removed by the compressive stress (ploughing mechanism) induced plastic deformation [20, 51].
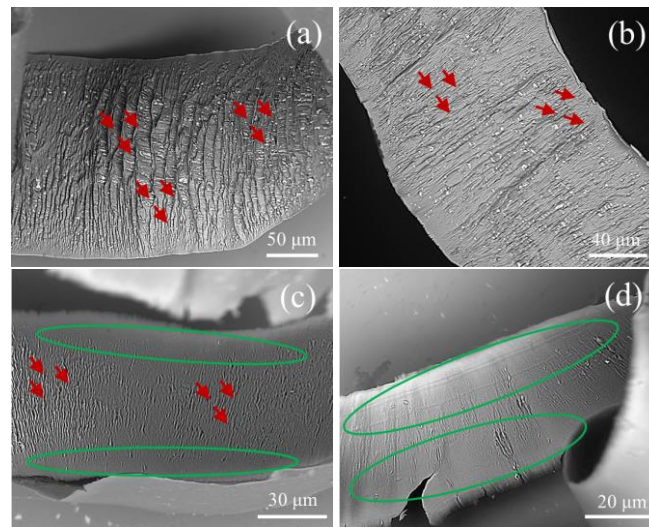

Fig. 10. The chip morphologies formed at the DoC of (a) 10 μm, (b) 5 μm, (c) 1 μm and 0.3 μm.

Through correlating the chip morphologies in Fig. 10 to the simulation results in Fig. 9 (b), the cutting mechanism transformation phenomenon from shearing (tensile stress) to ploughing (compressive stress) can be explained by the increase of the SF value with decreasing UDCT. To be more Specific, during diamond cutting, the workpiece material deforms in the cutting region and then flows on the tool rake face to form a chip. At tool tip, the SF value is very small, so more grains are involved in the cutting region to form the chip. Attributing to the large deformation resistance of grain boundary in this case, the chips breaks frequently at grain boundaries and the material is removed by tensile stress (shearing) in the shear band, resulting in the generation of lamella-like structures. In contrast, for region near the two sides of the cutting edge that have larger SF value, continuous chip formation mechanism is more prone to occur as the tool cuts within a single or only a few grains in this region. Besides, at very small UDCT, the equivalent rake angle of the diamond tool edge is negative, further resulting in the continuous plastic deformation of the material under high compressive stress (ploughing). According to [26], less hardening and lower resistance of grain boundary act on the dislocation movements during plastic deformation at lager SF, so compliable chips featuring smooth topographies are generated under the extrusion effect of diamond tool, which is the other reason for the cutting mechanism transformation with SF. Similar phenomenon is also observed in micro-cutting of aluminum alloys and pure copper [51].
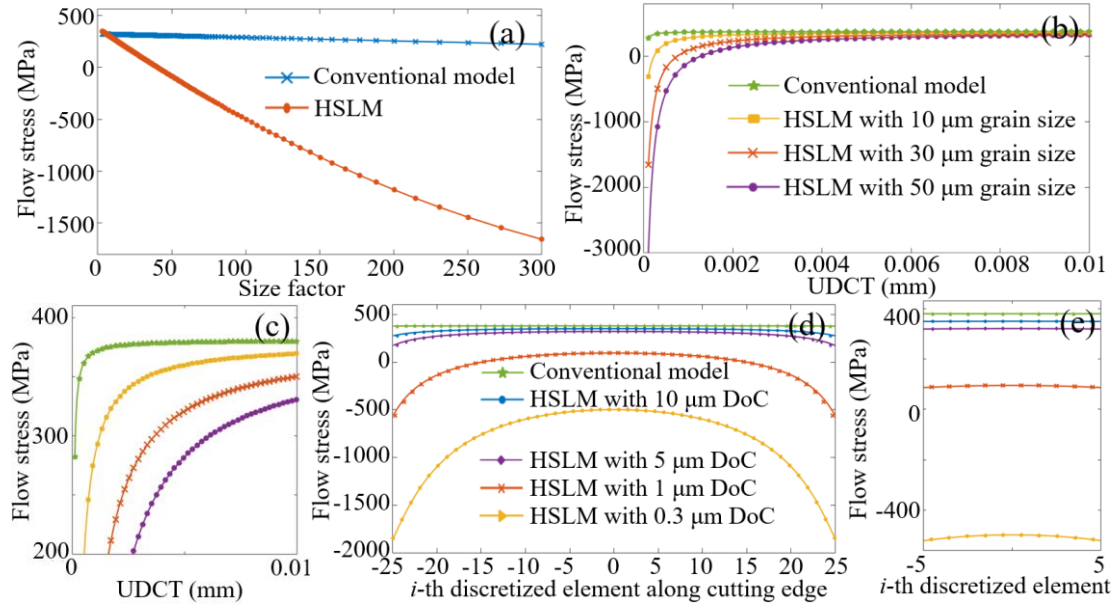
Fig. 11. The variation of the flow stress estimated by conventional model and HSLM with (a) size factor and (b) UDCT, (c) enlarged view of flow stress; (d) the variation of flow stress along cutting edge and (e) enlarged view of flow stress.

Noteworthy, conventional slip-line models used for micro/nano-cutting force estimation are generally developed by simply incorporating the effective rake angle into the macroscope slip-line models, and Johnson-Cook constitutive equation is normally employed to calculate flow stress. As shown in Fig. 11 (a), the flow stress calculated by the conventional slip-line models [13] are almost unchanged and remains in positive values (tensile stress) with the increase of SF, which cannot well explain the cutting mechanism transformation phenomenon in diamond cutting as observed in the different chip morphologies shown in Fig. 10. In comparison, by fully considering the equivalent negative rake angle as well as the microstructure and size effect, the proposed HSLM can well estimate the transition of flow stress from tensile (shearing) to compressive (ploughing) with the increase of SF, as shown in Fig. 11 (a). A further comparison of the proposed HSLM and conventional slip-line model in estimating the variation of flow stress with respect to UDCT and grain size is shown in Fig. 11 (b). It is seen that the flow stress calculated by HSLM increases from negative values (compressive stress) to positive values (tensile stress) with increase of UDCT, and is gradually approaching the flow stress calculated by conventional model at large UDCT. Besides, the flow stress calculated by the hybrid model decreases with the increase of grain size, due to the less grain boundary resistance during dislocation sliding for larger grains. A comparison of the strain-stress curves simulated by the conventional Johnson-Cook constitutive model and the proposed HSLM is shown in Fig. 12. It is seen that compared with Johnson-Cook model, HSLM can well capture the change of the constitutive relation from single crystal to polycrystal with decreasing SF. As illustrated in Fig. 9, smaller SF indicates that the material in the

deformation zone is more similar to polycrystal, so its strain-stress curve is closer to the curve of the

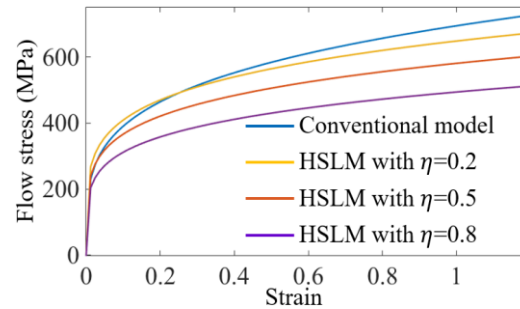Johnson-Cook model representing macro-mechanics properties.

Fig. 12. A comparison of the strain-stress curves of Johnson-Cook model and HSLM.

The change of the flow stress along cutting edge at different DoCs is also determined by the

proposed HSLM, as shown in Fig. 11 (d). It is learned that the flow stress changes from tensile to

compressive from the middle to the two sides of the cutting edge, and the portion of the compressive

stress increases with the decreases of DoC. This is caused by the trans-scale variation of UDCT and the

resulting large variation of SF along cutting edge as illustrated in Fig. 8 (a) and (d). Especially, only a

very small area on the tool tip features tensile stress at 1 μm DoC. When the DoC is as small as 0.3 μm,

most area of the cutting edge experience high compressive stress. The simulation results validate that the

proposed HSLM can well capture the UDCT-related cutting mechanism transition phenomenon in

diamond cutting, and the simulation results shown in Fig. 11 (d) are in good accordance with the observed

chip topographies shown in Fig. 10. The similar results of cutting mechanism transformation with

decreasing UDCT from other researchers also validate the effectiveness of proposed slip-line model [20].

4.3 Validation of trans-scale cutting force model

To validate the trans-scale force model, the estimated forces are compared with the measured forces

in diamond cutting of polycrystalline copper with the variation of Doc and grain size. Two polycrystalline

copper workpieces with different grain size of 24 μm and 52 μm are used in this study to investigate the

influence of grain size on cutting force. A large span of DoCs ranging from 0.3 μm to 15 μm were adopted

in the experiments, to sufficiently verify the general applicability of the proposed model. The parameters

related to material microstructure and size effect majorly include resolved grain size, size factor, critical

resolved shear stress coefficients and crystal orientation factor. The grain size is measured by an optical

microscope (BX60, Olympus corporation), and then size factor can be calculated according to its

definition. The coefficients related to the critical resolved shear stress are obtained by fitting the load-

stroke curve via upsetting experiments. Through summarizing the parameters used in Refs. [20, 29, 52],

the parameters relating to the physical characteristics of polycrystalline copper and Johnson-Cook constitutive equation are shown in Table 1. The remaining parameters listed in Table 2 are determined and optimized by generation algorithm, in which cutting forces with the DoC of 0.7 μm and 5 μm were used as learning material.

Table 1 Parameters related to material mechanics properties

D'	47.6	k_R	192
q	0.21	n	0.21
M	3.06	m	2
k	316 MPa	T_m	1084 °C
ρ	8.9 g/cm^3	T_0	25 °C
S	445 J/kg·°C	β'	0.35

Table 2 Parameters related to the analytical model

γ_0	0 °	C_0	7
v	30 mm/min	ζ	1.7
r_e	40 nm	a	0.134
β	15 °	b	0.211
r	3	j	0.6
μ_f	0.084	κ	7 °
μ_r	0.18	R	0.5 mm
N	50		

Table 3 A comparison of the measured forces and estimated forces for different grain sizes and DoCs

DoC (μm)	Forces for 24 μm grain size	Forces for 52 μm grain size
0.3		

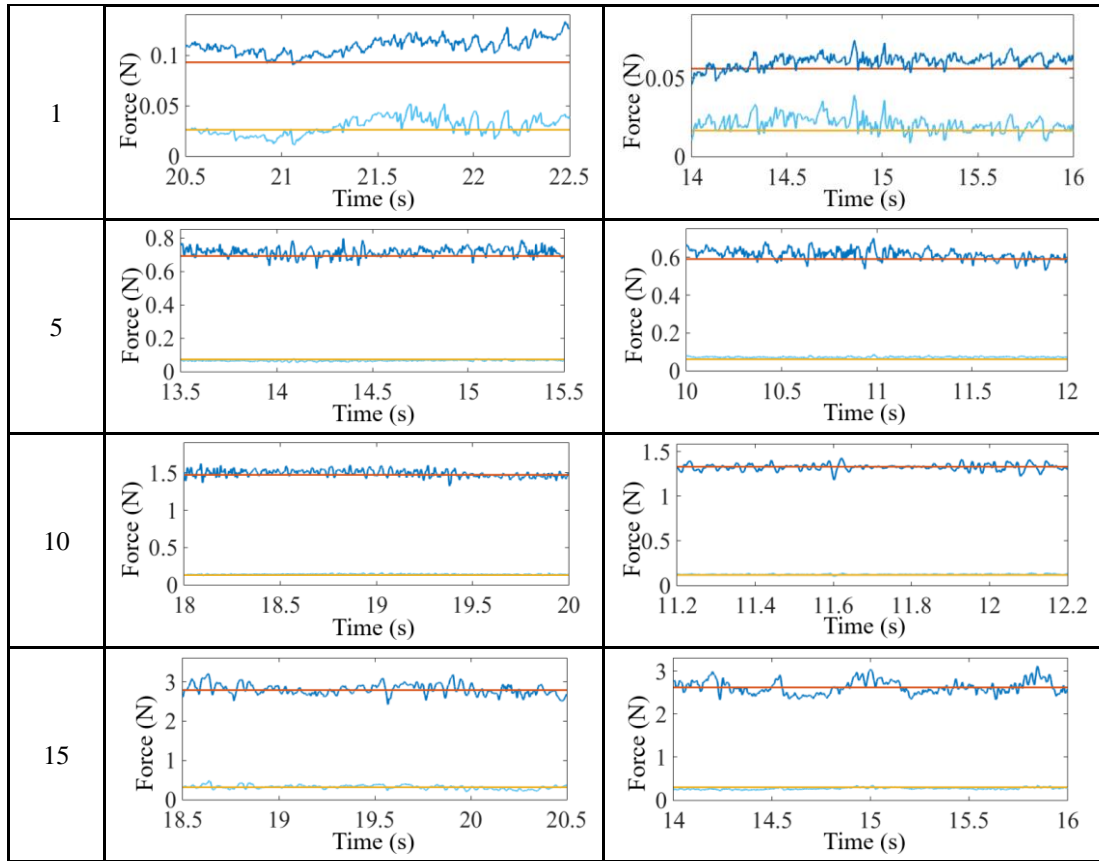|		
1		
5		
10		
15		
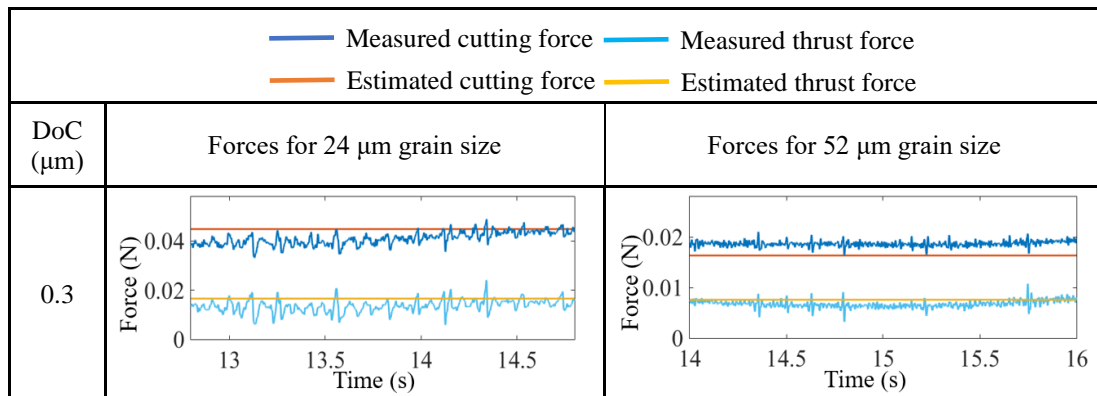
Table 3 compares the estimated and measured forces under different DoCs and different grain sizes. The high-frequency noise is filtered by a low-pass filter of 130 Hz to make the signal smooth. It is interesting to observe that the cutting force signal becomes increasingly oscillated with the decrease of DoC, which validates the prominence of the influence of microstructure, such as crystallographic anisotropy and grain boundary, and ploughing effect on cutting force in micro/nano-cutting scale. In contrast, the statistical uniformity of the microstructure in macroscope cutting under large DoCs suppresses the oscillations of cutting forces. As shown in Table 3, it is also observed that the cutting forces for the larger grain size of 52 μm is a bit smaller than that for smaller grain size of 24 μm even under the same DoC. This is because the larger the grain size, the smaller the flow stress in the cutting region, as illustrated by the simulation results shown in Fig. 11 (b).
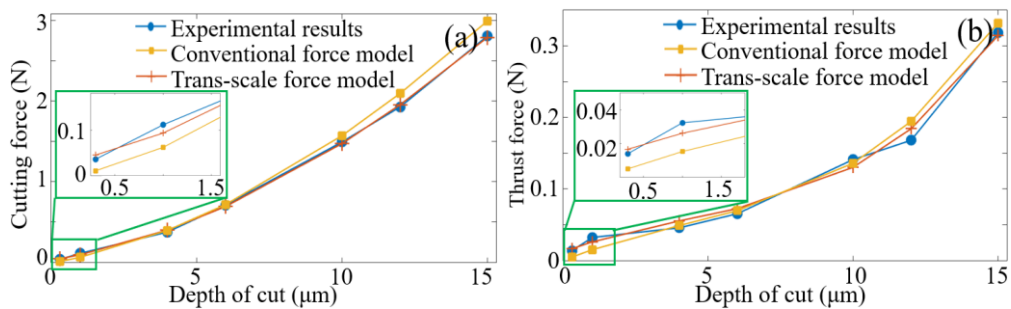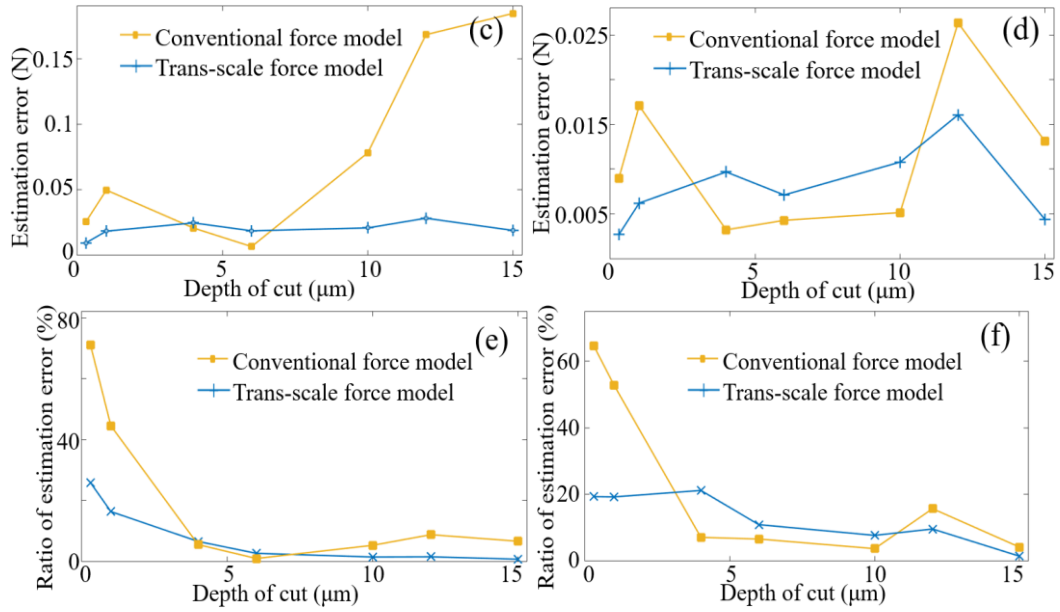
Fig. 13. A comparison of experimental and estimated results for the (a) cutting forces and (b) thrust forces, the estimation error of (c) cutting forces and (d) thrust forces and the ratio of estimation error of (e) cutting forces and (f) thrust forces for 24 μm grain size.

To validate the advantage of the proposed trans-scale cutting force model, the simulation of cutting force using conventional diamond cutting force model [13] is also carried out for comparison. A graphical trend of the estimated and measured results for the cutting force and thrust force is shown in Fig. 13 (a) and Fig. 13 (b), respectively, and the corresponding modelling error is shown in Fig. 13 (c) and Fig. 13 (d), respectively. The experimental results presented in Fig. 13 (a) and (b) are the mean arithmetic values of the measured cutting forces. It is seen that compared with the conventional model, the simulated results of the proposed trans-scale cutting force model are in better accordance with the experimental results for both cutting forces and thrust forces even under a big change of DoC from 0.3 μm to 15 μm. For the proposed model, the maximum modelling error of the cutting force and thrust force are very small at 0.03 N and 0.016 N, respectively. This is attributed to the full consideration of the equivalent negative rake angle, microstructure and size effect in the proposed HSLM, so more coefficients relating to material micro-mechanics properties are in involved to improve the estimation accuracy. In contrast, the modelling error of conventional model obviously increase when the DoC is lower than 4 μm or larger than 10 μm, and the maximum modelling error of cutting force and thrust force reach about 0.18 N and 0.026 N, respectively. Considering the very large variation of the cutting force values at different DoCs, the relative error defined as the ratio of modelling error to the measured force is also employed in this study to evaluate the estimation accuracy. As shown in Fig. 13 (e) and (f), for the conventional force model, the relative error greatly increases with the decrease of DoC, especially

reaching up to nearly 70% at a small DoC of 0.3 μm. The cause of the large modelling error of the conventional model is that the macroscopic slip-line model based on Johnson-Cook equation cannot accurately calculate the high compressive stress at small UDCT, as illustrated in Fig. 11 (b). In contrast, the relative error of proposed model is less than 20% for both cutting force and thrust force. Similar graphic trend of the cutting force and modelling error are also obtained for the workpiece with grain size of 52 μm, as shown in Fig. 14. The good agreement of the estimated and experimental results at different DoCs validates the effectiveness and advantage of proposed model in estimating trans-scale cutting forces for different grain sizes.
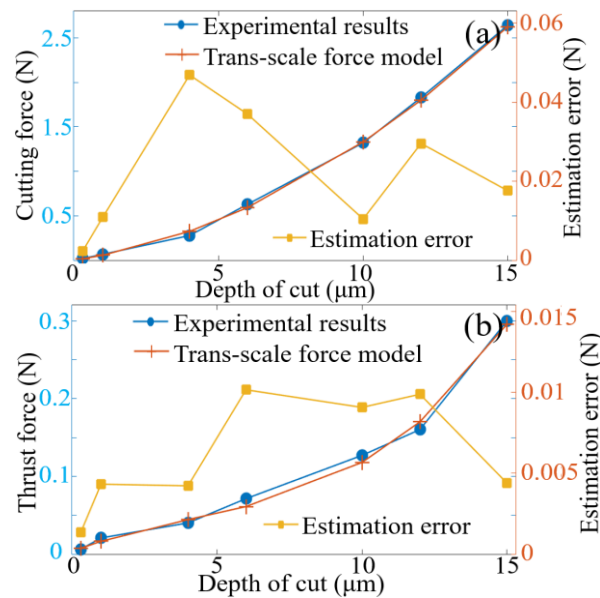

Fig. 14. A comparison of the experimental and estimated results of the (a) cutting forces and (b) thrust forces for 52 μm grain size.

Conclusions

This study proposes an analytical trans-scale cutting force model for diamond cutting of polycrystalline metals with the full consideration of the trans-scale variation of undeformed chip thickness (UDCT) along cutting edge and the resulting transformation of cutting mechanism from shearing to ploughing. By dividing the workpiece into two layers, namely surface and inner layers, a hybrid slip-line model (HSLM) is developed to calculate the flow stress in cutting region. The influence of grain size, grain boundary and crystal orientation on the flow stress is also involved in the HSLM based on crystal plastic theory. Then, the normal cutting force and frictional cutting force are determined by analyzing the stress distribution and the frictional states in the secondary deformation zone using a tool-chip contact model. Besides, the rubbing force induced by elastic recovery is determined by assuming its value is proportional to the tool-workpiece interference volume. Finally, discrete and

summation methods is employed to solve the variation of cutting force along cutting edge for each discrete elements. The proposed model is experimentally validated by diamond cutting polycrystalline copper with different grain sizes, and the following conclusions can be drawn:

- The novelty of the proposed HSLM lies in its capability to determine the contribution of microstructure and size effect on the flow stress in the cutting region. By correlating the simulation results and the formed chip morphologies under different depths of cut, it has been demonstrated that the proposed HSLM is able to capture the transformation of flow stress from tensile (shearing) to compressive (ploughing) with decreasing UDCT.

- The estimated cutting forces of the proposed model agree well with the experimental results that smaller cutting forces are generated for larger grain size. According to the proposed HSLM, at larger grain size, the influence of grain size effect described by size factor becomes prominent and the less grain boundaries are involved in the cutting region to resist dislocation sliding, thereby resulting in less flow stress and smaller cutting force.

- Compared with conventional force models developed based on Johnson-Cook equation, the proposed trans-scale cutting force model presents an obviously improved estimation accuracy even under a large variation of DoC from 0.3 μm to 15 μm. This is attributing to the uniqueness of the proposed force model to estimate the high compressive stress at very small UDCT and to capture the transformation phenomenon of flow stress with increasing UDCT.

- Attributing to the discretization method, the proposed force model can estimate the distribution of flow stress and cutting force along cutting edge. The model demonstrate that the flow stress decreases from tool tip to the two sides of the cutting edge, and the ratio of the region covered by compressive stress increases with decreasing DoC. This results in the variation of chip morphology from lamella-like structures in the middle to the smooth and thin shape near the two sides.

References

[1] S. Zhang, Y. Zhou, H. Zhang, Z. Xiong, S. To, Advances in ultra-precision machining of micro-structured functional surfaces and their typical applications, International Journal of Machine Tools and Manufacture, (2019).

[2] Z. Sun, S. To, S. Wang, J. Du, Development of self-tuned diamond milling system for fabricating infrared micro-optics arrays with enhanced surface uniformity and machining efficiency, Optics Express, 28 (2020) 2221-2237.

[3] X. Jing, R. Lv, Y. Chen, Y. Tian, H. Li, Modelling and experimental analysis of the effects of run out, minimum chip thickness and elastic recovery on the cutting force in micro-end-milling, International Journal of Mechanical Sciences, 176 (2020) 105540.

[4] Y. Chen, J. Wang, Q. An, Mechanisms and predictive force models for machining with rake face textured cutting tools under orthogonal cutting conditions, International Journal of Mechanical Sciences, 195 (2020) 106246.

[5] G. Yuan, R. Sun, J. Leopold, Analysis of Cutting Stability in Vibration Assisted Machining Using Ananalytical Predictive Force Model, Procedia CIRP, 31 (2015) 515-520.

[6] Y.L. Chen, Y. Cai, K. Tohyama, Y. Shimizu, S. Ito, W. Gao, Auto-tracking single point diamond cutting on non-planar brittle material substrates by a high-rigidity force controlled fast tool servo, Precision Engineering, 49 (2017) 253-261.

[7] Y. Dai, G. Zhang, T. Luo, Q. Luo, Centre cone generation and its force performance in single-point diamond turning, International Journal of Mechanical Sciences, 184 (2020).

[8] S. Wang, S. Xia, H. Wang, Z. Yin, Z. Sun, Prediction of surface roughness in diamond turning of Al6061 with precipitation effect, Journal of Manufacturing Processes, 60 (2020) 292–298.

[9] P. Huang, B.W. Lee, Cutting force prediction for ultra-precision diamond turning by considering the effect of tool edge radius, International Journal of Machine Tools and Manufacture, 109 (2016) 1-7.

[10] X. Zhang, T. Yu, J. Zhao, An analytical approach on stochastic model for cutting force prediction in milling ceramic matrix composites, International Journal of Mechanical Sciences, 168 (2020) 105314.

[11] J. Weng, K. Zhuang, C. Hu, H. Ding, A PSO-based semi-analytical force prediction model for chamfered carbide tools considering different material flow state caused by edge geometry, International Journal of Mechanical Sciences, 169 (2019) 105329.

[12] J.Q. Lin, J.G. Han, X.Q. Zhou, Z.P. Zhao, M.M. Lu, Study on predictive model of cutting force and geometry parameters for oblique elliptical vibration cutting, International Journal of Mechanical Sciences, 117 (2016) 43-52.

[13] Z. Zhu, S. To, W.-L. Zhu, P. Huang, X. Zhou, Cutting forces in fast-/slow tool servo diamond turning of micro-structured surfaces, International Journal of Machine Tools and Manufacture, 136 (2019) 62-75.

[14] S. Wojciechowski, M. Matuszak, B. Powałka, M. Madajewski, R.W. Maruda, G.M. Królczyk, Prediction of cutting forces during micro end milling considering chip thickness accumulation, International Journal of Machine Tools and Manufacture, 147.

[15] M. Wan, D.Y. Wen, Y.C. Ma, W.H. Zhang, On material separation and cutting force prediction in micro milling through involving the effect of dead metal zone, International Journal of Machine Tools and Manufacture, 146 (2019) 103452.

[16] D. Przestacki, T. Chwalczuk, S. Wojciechowski, The study on minimum uncut chip thickness and cutting forces during laser-assisted turning of WC/NiCr clad layers, The International Journal of Advanced Manufacturing Technology, 91 (2017) 3887-3898.

[17] Z. Fu, X. Chen, J. Mao, T. Xiong, An analytical force mode applied to three-dimensional turning based on a predictive machining theory, International Journal of Mechanical Sciences, 136 (2018) 94-105.

[18] G. Li, S. Li, K. Zhu, Micro-milling force modeling with tool wear and runout effect by spatial analytic geometry, The International Journal of Advanced Manufacturing Technology, 107 (2020) 631-643.

[19] M.E. Merchant, Mechanics of the metal cutting process. I. Orthogonal cutting and a type 2 chip, Journal of applied physics, 16 (1945) 267-275.

[20] M.A. Rahman, M. Rahman, A.S. Kumar, Modelling of flow stress by correlating the material grain size and chip thickness in ultra-precision machining, International Journal of Machine Tools & Manufacture, (2017) S0890695517301177.

[21] R. Ebrahimi, E. Shafiei, Mathematical Modeling of Single Peak Dynamic Recrystallization Flow Stress Curves in Metallic Alloys, InTech, 2012.

[22] X. Long, B. Hu, Y. Feng, C. Chang, M. Li, Correlation of microstructure and constitutive behaviour of sintered silver particles via nanoindentation, International Journal of Mechanical Sciences, 161-162 (2019) 105020.

[23] J.Q. Ran, M.W. Fu, A hybrid model for analysis of ductile fracture in micro-scaled plastic deformation of multiphase alloys, International Journal of Plasticity, 61 (2014) 1-16.

[24] A. Prasitthipayong, S.J. Vachhani, S.J. Tumey, A.M. Minor, P. Hosemann, Indentation size effect in unirradiated and ion-irradiated 800H steel at high temperatures, Acta Materialia, 144 (2017).

[25] Y.C. Kim, E.J. Gwak, S.M. Ahn, N.R. Kang, H.N. Han, J.I. Jang, J.Y. Kim, Indentation size effect for spherical nanoindentation on nanoporous gold, Scripta Materialia, 143 (2018) 10-14.

[26] G.Y. Kim, N. Jun, K. Muammer, Modeling of the Size Effects on the Behavior of Metals in Microscale Deformation Processes, Journal of Manufacturing Science & Engineering, 129 (2007) 470-476.

[27] N. Chen, M. Chen, C. Wu, X. Pei, J. Qian, D. Reynaerts, Research in minimum undeformed chip thickness and size effect in micro end-milling of potassium dihydrogen phosphate crystal, International Journal of Mechanical Sciences, (2017) 387-398.

[28] X. Lai, L. Peng, P. Hu, S. Lan, J. Ni, Material behavior modelling in micro/meso-scale forming process with considering size/scale effects, Computational Materials Science, 43 (2008) 1003-1009.

[29] G. Zhang, J. Ran, S. To, X. Wu, P. Huang, M.P. Kuz'min, Size effect on surface generation of multiphase alloys in ultra-precision fly cutting, Journal of Manufacturing Processes, 60 (2020) 23-36.

[30] D. Germain, G. Fromentin, G. Poulachon, S. Bissey-Breton, From large-scale to micromachining: A review of force prediction models, Journal of Manufacturing Processes, 15 (2013) 389-401.

[31] N. Fang, I. Jawahir, P. Oxley, A universal slip-line model with non-unique solutions for machining with curled chip formation and a restricted contact tool, International Journal of Mechanical Sciences, 43 (2001) 557-580.

[32] Q. Ke, D. Xu, D. Xiong, Cutting zone area and chip morphology in high-speed cutting of titanium alloy Ti-6Al-4V, Journal of Mechanical Science and Technology, 31 (2017) 309-316.

[33] H. Ren, Y. Altintas, Mechanics of Machining With Chamfered Tools, Journal of Manufacturing ence and Engineering, 122 (2000) 650-659.

[34] C. Hu, K.J. Zhuang, J. Weng, X.M. Zhang, Thermal-mechanical model for cutting with negative rake angle based on a modified slip-line field approach, International Journal of Mechanical ences, 164 (2019) 105167-105167.

[35] P.L.B. Oxley, H.-T. Young, The mechanics of machining: an analytical approach to assessing machinability, in, Chichester, England: Ellis Horwood Publisher, 1990.

[36] P. Oxley, W. Hastings, Predicting the strain rate in the zone of intense shear in which the chip is formed in machining from the dynamic flow stress properties of the work material and the cutting conditions, Proceedings of the Royal Society of London. A. Mathematical and Physical Sciences, 356 (1977) 395-410.

[37] L. Peng, X. Lai, H.J. Lee, J.H. Song, J. Ni, Analysis of micro/mesoscale sheet forming process with uniform size dependent material constitutive model, Materials Science & Engineering A, 526 (2009) 93-99.

[38] Z. Sun, S. To, S. Wang, An analytical force model for ultra-precision diamond sculpturing of micro-grooves with textured surfaces, International Journal of Mechanical Ences, 160 (2019) 129-139.

[39] M.P. Vogler, S.G. Kapoor, R.E. DeVor, On the modeling and analysis of machining performance in micro-endmilling, Part II: Cutting force prediction, Journal of manufacturing science and engineering, 126 (2004) 695-705.

[40] Z. Wang, J. Zhang, Z. Xu, J. Zhang, T. Sun, Crystal anisotropy-dependent shear angle variation in orthogonal cutting of single crystalline copper, Precision Engineering, 63 (2020) 41-48.

[41] M. Sakkaki, F.S. Moghanlou, M. Vajdi, F. Pishgar, M.S. Asl, The effect of thermal contact resistance on the temperature distribution in a WC made cutting tool, Ceramics International, 45 (2019).

[42] V. Kuznetsov, Y.K. Shlyk, Y.A. Vedernikova, R.Y. Nekrasov, I. Kokorin, Thermoelectric model of the cutting process, Russian Engineering Research, 40 (2020) 518-521.

[43] G. Boothroyd, Temperatures in Orthogonal Metal Cutting, ARCHIVE Proceedings of the Institution of Mechanical Engineers 1847-1982 (vols 1-196), 177 (1996) 789-810.

[44] Z. Wang, M. Rahman, Y. Wong, X. Li, A hybrid cutting force model for high-speed milling of titanium alloys, CIRP annals, 54 (2005) 71-74.

[45] A. Moufki, A. Molinari, D. Dudzinski, Modelling of orthogonal cutting with a temperature dependent friction law, Journal of the Mechanics and Physics of Solids, 46 (1998) 2103-2138.

[46] F. Fang, F. Xu, Recent Advances in Micro/Nano-cutting: Effect of Tool Edge and Material Properties, Nanomanufacturing & Metrology, (2018).

[47] S. Bahi, M. Nouari, A. Moufki, M.E. Mansori, A. Molinari, Hybrid modelling of sliding–sticking zones at the tool–chip interface under dry machining and tool wear analysis, Wear, 286-287 (2012) 45-54.

[48] J.H. Ko, Time domain prediction of milling stability according to cross edge radiuses and flank edge profiles, International Journal of Machine Tools & Manufacture, 89 (2015) 74-85.

[49] M. Malekian, S.S. Park, M.B.G. Jun, Modeling of dynamic micro-milling cutting forces, International Journal of Machine Tools & Manufacture, 49 (2009) 586-598.

[50] H., Wang, and, S., To, and, C.Y., Chan, and, C.F., Elastic strain induced shear bands in the microcutting process - ScienceDirect, International Journal of Machine Tools & Manufacture, 50 (2010) 9-18.

[51] Z. Wang, J. Zhang, Z. Xu, J. Zhang, H. Ul Hassan, G. Li, H. Zhang, A. Hartmaier, F. Fang, Y. Yan, Crystal plasticity finite element modeling and simulation of diamond cutting of polycrystalline copper, Journal of Manufacturing Processes, 38 (2019) 187-195.

[52] G.R. Johnson, A constitutive model and data for materials subjected to large strains, high strain rates, and high temperatures, Proc. 7th Inf. Sympo. Ballistics, (1983) 541-547.